Computers & Graphics xxx (xxxx) xxx

Contents lists available at ScienceDirect

Computers & Graphics

journal homepage: www.elsevier.com/locate/cag

Special Section on CAD & Graphics 2019

Modeling fractures and cracks on tree branches

Q1 Liuming Yang, Meng Yang*, Gang Yang

School of Information Science and Technology, Beijing Forestry University, Beijing, PR China

ARTICLE INFO

Article history:
Received 9 March 2019
Accepted 23 March 2019
Available online xxx

Keywords:
Simulation
Procedural modeling
Fractures
Cracks
Wood
Branch breaking

ABSTRACT

Wood is a complex biological material. Due to the anisotropy of wood, the difference in the structure and physical-mechanical properties of different tree species, and the irregularity and complexity of the internal structure of tree branches, it is challenging to model wood fractures caused by natural disasters and man-made damage. In this paper, we propose a user-controllable procedural modeling algorithm simulating the fractures based on the theory of wood science and wood fracture mechanics. It can also simulate cracks caused by wood shrinkage. The roughness of the corresponding area on the fracture surface is adjusted by setting the parameters of different material properties of pith, heartwood, sapwood, and bark; when the branches are broken, the fracture surface of the wood area under tension is treated as uneven and full of spines, and the pressure part is treated as a more regular section; the wood composed of different types of plant cells is represented by a group of particles. Various realistic cracks on wood fracture surface can be simulated by setting different strength and shrinkage rate in axial, radial and tangential direction. We illustrate our approach with various models from several tree species. Experimental results indicate that our approach can be used to model fractures and cracks on tree branches efficiently and realistically.

1. Introduction

At present, there are numerous tree dynamic simulation methods and material fracture simulation algorithms in computer graphics, but there are few reasonable and effective simulation algorithms specifically for wood fractures. Wood is one of the four major materials (plastics, cement, steel, wood), and trees are one of the essential elements of nature scenes. In addition, wood has porous, anisotropic and viscoelastic properties, as well as the diversity of appearance and physical-mechanical properties for different tree species, the irregularity and complexity of wood structure. In previous works, some simple simulation results are obtained by simplifying many conditions. So currently the models of broken branches needed in-game animation or movie special effects are still manually modeled by artists. In the simulation of realistic natural scenes, it often includes the simulation of some natural disasters, such as storms, hail, and snowstorm. These natural disasters cause damage to trees, such as tree branches were broken by a hurricane, accumulated snow and rime. There are also man-made damage to trees caused by fierce fighting in some animation scenes. Fig. 1 shows the complex effect of a branch breaking. Therefore, the simulation of the irregular fracture surface of branches is of great significance. The goal of this work is to quickly generate reasonable and realistic wood fracture models.

Our algorithm is inspired by wood science literature. We propose a procedural algorithm, depending on a set of easily tunable parameters, to set the properties of basic features of tree branch's fracture surface. So, artists can directly tune the parameters of our algorithm. Our algorithm provides parameters to set the delamination effect of the fracture surface to simulate the phenomenon of high and low delamination of wood fracture surface due to the extremely fragile wood ray cells arranged radially in the wood cells. At the same time, our algorithm provides parameters to control the roughness of the fracture surface and the number and length of fiber thorns. Combined with the delamination effect, we can simulate the phenomenon that when a branch bends or breaks, the outside side of the branch is subjected to tensile internal force, resulting in uneven and spiny ductile fracture zone and the relatively flat zone inside the fracture surface. We also give a procedural method to generate cracks on the cross-section of wood both in the radial direction and tangential direction. Fig. 2 shows the process of quickly generating a model of a broken branch with our method.

The main contributions of our work can be described as follows:

- We propose a user-controllable method to simulate the complex appearance of breaking tree branches more realistically

* Corresponding author.
E-mail address: yangmeng@bjfu.edu.cn (M. Yang).

https://doi.org/10.1016/j.cag.2019.03.006
0097-8493/

Fig. 1. A photograph of a broken branch. It can be clearly seen that the xylem part of the branch is composed of a plurality of fibers, and the fibers are distorted and deformed.

than previous methods do. By inputting a set of parameters about the intuitive appearance features of branch fractures, different broken branches models can be generated automatically.
- To our knowledge, it is an early attempt to apply the theory of wood science and wood fracture mechanics to the simulation of branches breaking.
- We establish a relation between the physical-mechanical properties of wood and the height of the fracture surface of branches.

2. Related work

In previous works of computer graphics, there were many studies on tree simulation: from the modeling of trees to the interaction of trees with various environmental factors (external forces, wind, rain, hail). In wood science, many physical-mechanical properties of wood have been studied in detail from the perspective of materials science. In wood fracture mechanics, there are many studies on bending, fracture, and wood fracture characteristics of wood.

2.1. Tree modeling and animation algorithm

In the early days of tree modeling research, some procedural modeling methods were usually used. For example, Weber and Penn [1] propose an algorithm for creating tree models quickly, focusing on the overall geometry of a tree rather than strictly following the principles of botany. With the development of 3D scanning technology, 3D point cloud-based tree modeling methods have emerged to produce 3D tree models [2–5]. Livny et al. [3,4] propose methods for automatically generating realistic tree models from scanned tree 3D point clouds based on pre-generated tree classification information. It is capable of reconstructing multiple overlapping tree models automatically. There are also many animation researches on tree growth [6,7]. Kratt et al. [7] propose a simulation method for cambial growth and cracks on bark. Modeling wood fractures and cracks is still a challenging task.

2.2. Interactive simulation algorithm of trees and environment

Different representations of botany models have different advantages and disadvantages when simulating the interaction between trees and environmental factors. Diener et al. [8] propose a method for real-time simulation of complex scenes that contain thousands of trees under user-controlled wind load. Quigley et al. [9] propose an interactive real-time animation method based on representing tree models as articulated rigid bodies. Yang and Wu [10] simulate the interaction between tree branches and raindrops. Wang et al. [11] propose a method of automatically setting material properties of tree models based on biomechanics according to the power law relationship between vibration frequency and the length and diameter of branches. A biologically reasonable simulation method for tree combustion is in research [12]. Simulating wood fractures can be an extension of the above work.

2.3. Fractures modeling and animation in graphics

The simulations of fractures in computer graphics usually consider material as an ideal brittle material or isotropic material. O'Brien et al. [13] propose a method that calculates crack's the propagation direction by the stress tensor on the finite element model; The method's results depend on the elastic deformation range, plastic deformation range and deformation limit of each element. Pfaff et al. [14] propose a method for adaptive crack propagation on thin-film models. Chen et al. [15] propose a method that is easy for users to design and control the effect of the cross-section. The low-resolution fracture surface mesh is refined into high-resolution, detail-rich fractures based on the material strength field set by users. Desbenoit et al. [16] propose a purely graphic method for modeling cracks and fractures by mapping editable 2D curve patterns onto three-dimensional models. For the method of simulating branch breakage or simulating wood fracture, the previous methods neglect the anisotropy and structural properties of wood, approximated the branch fracture section to a smooth elliptical surface or used noise to simulate the strength of the branch section, lacking rationality and realism.

2.4. Wood science and wood fracture mechanics

Researches on the internal structure and the physical-mechanical properties of wood have been studied in detail in many wood science literature [17]. The Institute of Wood Industry of the Chinese Academy of Forestry [18] test 23 physical-mechanical properties of 342 tree species, including latewood rate, air dry density, dry shrinkage coefficient, compressive strength, shear strength, tensile strength, hardness, etc. Jiang and Peng [19] test and analyze the wood anatomical properties and 10 physical-mechanical properties of 458 species of wood. Yao [20] uses scanning electron microscopy to observe the internal structure of wood

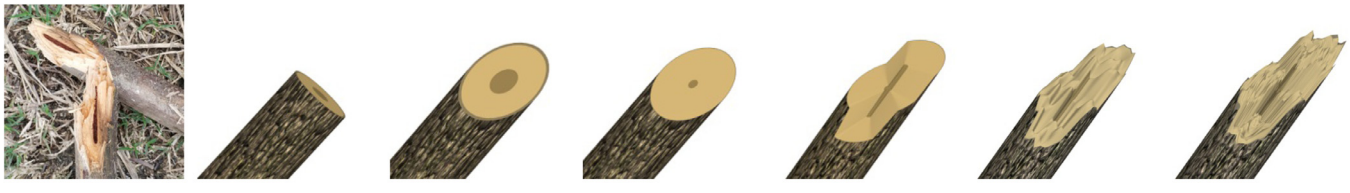

Fig. 2. The process of simulating broken branches using the method of this paper. (a)A photograph of broken branches. (b) The initial shape of the branch model. (c) Set the angle of inclination of the fracture surface. (d) Set the proportion of phloem and pith. (e) Set the layering effect of the fracture surface. (f) Add the appropriate Perlin noise to the height of vertices on the fracture surface. (g) Add the appropriate white noise to the height of vertices on the fracture surface.

Please cite this article as: L. Yang, M. Yang and G. Yang, Modeling fractures and cracks on tree branches, Computers & Graphics, https://doi.org/10.1016/j.cag.2019.03.006

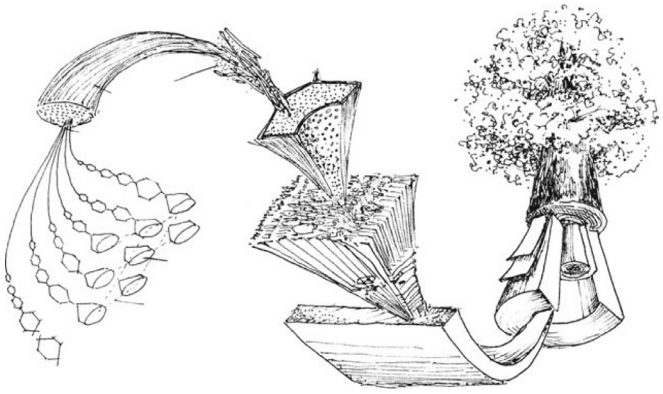

Fig. 3. The sketch of wood structure.

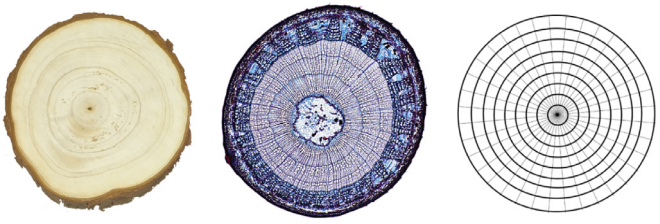

Fig. 4. (a) A photograph of the cross-section of wood. (b) A sketch shows the microstructure of wood. (c) The mesh structure of the cross-section of a tree branch model.

in 127 tree species, and can clearly observe the arrangement of cells.

Wood damage and fractures are a complex multi-level and multi-stage process. Vasic et al. [21] propose numerical models for wood fracture mechanics using finite element techniques. The book [22] shows the researches on the fracture and destruction behavior of wood and bamboo that clearly describes the mechanical characteristics. It shows three stages in the process of wood bending: I. linear elastic deformation stage; II. nonlinear deformation stage; III. ductile fracture stage. Wood breakage is accompanied by the accumulation and release of energy in the material.

The fracture cracks of wood show obvious fractal characteristics. Crack regions with different sizes have statistically self-similar characteristics in morphology and combination distribution. Khennane et al. [23] propose a numerical model to predict the ductile damage in tensile and bending tests on timbers. Through their experimental results, the damage state of the wood at various stages of the fracture can be clearly seen. Fei and Zhang [24] use the counting box dimension method to describe the fractal characteristics of the crack stress field. Many studies [25,26] scan the morphology of wood fractures with CT technology and analyze the morphological characteristics of wood fractures with image processing techniques. It has been found that the fractal dimension values of the fractured sections of woods with different tree species are significantly different.

This is an exciting work that applies these knowledge to modeling work in graphics.

3. Modeling fractures on tree branches

3.1. Fracture surface representation based on wood structure

Wood is different from homogeneous or isotropic materials such as metals and plastics. As shown in Figs. 3 and 4, the macroscopic feature of the wood is having annual rings on cross-section.

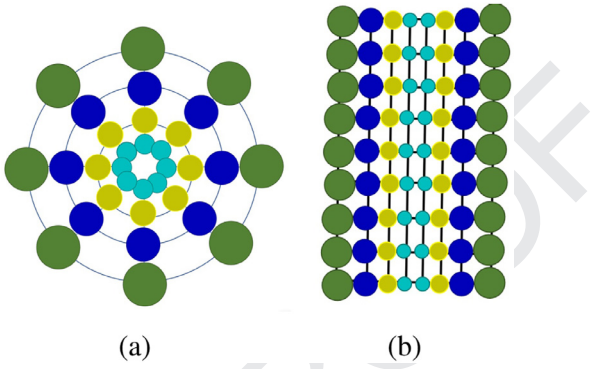

Fig. 5. Cross-section and longitudinal section of particle-based presentation of a branch. A branch is discretized into several groups of particles connected by spring-mass system (black lines), with color denoting particle type (dark green - phloem, navy blue sapwood, yellow heartwood, cyan pith). (For interpretation of the references to color in this figure legend, the reader is referred to the web version of this article.)

From a microscopic point of view, wood is composed of a variety of plant cells with different functions. The arrangement, shape, and size of the cells of the medulla, xylem, and phloem are greatly different, as shown in Fig. 4(b). Although many works [27–29] have studied and simulated the various shapes and arrangement of plant cells, accurate modeling of every plant cell in wood is still a tough task. In our work, we simply represent branches by connected particles, as shown in Fig. 5. Each particle inside of wood is connected to the other six. The left and right particles can be regarded as wood cells located in the same annual ring with the center particle. The above and below particles can be considered as wood cells located in the same wood fiber bundle with the center particle. The inner, center and outer particles can be considered as cells on the same wood ray in some condition. The fracture surface of the branch model is composed of circles. The innermost circle is composed of a circle of triangles. Other than these, other outer rings are composed of circles of quadrangles. The number of concentric circles set in the experiment was 40, and the number of sectors was 40. It will generate 1600 particles on each layer in the axial direction of the branches. When the larger the radius of the simulated branch, the finer cross-section is required, so the sum of concentric circles and the number of sectors should be set bigger.

3.2. Different material properties on the cross-section of wood

Wood structure can be roughly divided into bark, phloem, xylem and pith from the outer layer to the inner layer, as shown in Fig. 6. The non-uniformity of wood on the cross-section is characterized by different material properties of the core, heartwood, sapwood, phloem, and bark. Our algorithm provides ν_{pith}, $\nu_{heartwood}$ and ν_{phloem} parametrize the proportion of pith, heartwood and phloem respectively. The number of concentric circles on the cross-section is N_{ring}, and the concentric circle position of the particle i is R_i. When $R_i \leq N_{ring}\nu_{pith}$, the particle is located in pith portion. When $N_{ring}\nu_{pith} < R_i \leq N_{ring}(\nu_{pith} + \nu_{heartwood})$, the particle is located in heartwood. When $N_{ring}(\nu_{pith} + \nu_{heartwood}) < R_i \leq N_{ring}(1 - \nu_{phloem})$, the particle is located in sapwood. When $N_{ring}(1 - \nu_{phloem}) < R_i < N_{ring}$, the particle is located in phloem. When $R_i = N_{ring}$, the particle is located in bark.

According to wood science, xylem can be divided into heartwood and sapwood; the lignin content of the heartwood is high while the cellulose content is low. So, the color, density and mechanical properties of heartwood are different from those of sapwood, and the fracture surface effects are also very different. In order to obtain a more detailed and irregular fracture surface, our

Please cite this article as: L. Yang, M. Yang and G. Yang, Modeling fractures and cracks on tree branches, Computers & Graphics, https://doi.org/10.1016/j.cag.2019.03.006

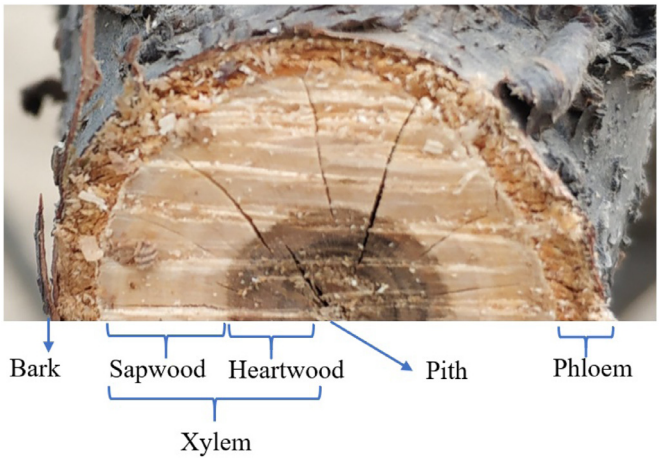

Fig. 6. Wood structure can be divided into bark, phloem, xylem and pith from the outer layer to the inner layer.

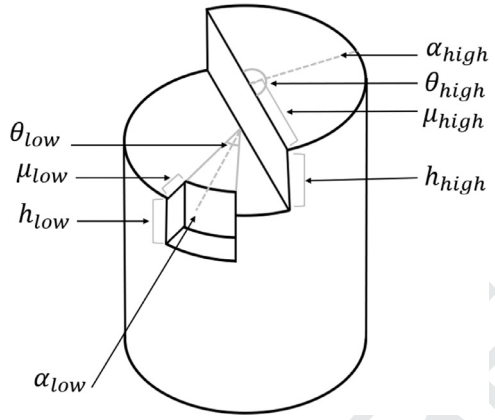

Fig. 7. Explanation diagram for parameters setting up fracture surface layering.

algorithm provides λ, β to set the roughness of the different parts of wood for scaling Perlin noise, and white noise was added. By adjusting the parameters for Perlin noise, a large number of broken branch models that look more photorealistic can be quickly generated.

$$H_j += \lambda_{phloem} Perlin(\beta_{phloem} x_j, \beta_{phloem} y_j), Perlin() \in [0, 1] \quad (1)$$

where H_j is the height of vertex j; vertex j is on the particle i; and Perlin() is a function that generates Perlin noise.

3.3. Wood ray

Wood ray is radially outwardly arranged from the center to the bark on the cross-section view of wood. It is in the xylem, used for laterally diverting nutrients and moisture. Wood ray is mainly composed of thin-walled cell tissue, which is relatively fragile, and wood is easily cracked along the ray under stress. As a result, when branches are broken, the shape often appears as a fan-shaped portion with an upper, middle and lower layer, as shown in Fig. 16(a), which is considered in our principles of fracture surface. Users can obtain the obvious layered effect by setting the angle occupied by a certain sector on the fracture section and the orientation and height of the sector.

Our algorithm provides h_{high} and h_{low} for setting the relative heights of the high and low layers compared with the middle layer, and α_{high}, θ_{high}, μ_{high}, α_{low}, θ_{low}, μ_{low}, respectively parametrize the direction, angle and rings of the high layer sector and low layer sector, as shown in Fig. 7.

Fig. 8. A photograph of broken branches of Amygdalus triloba f. multiplex. The fracture surface is clearly divided into a relatively flat zone and another zone covered with small thorns.

When the vertex j is located in a high layer, its height increases by h_{high}, and when the vertex is in the low layer, its height decreases by h_{low}. When:

$$\frac{(\alpha_{high} - \theta_{high}/2)N_{sec}}{360} \le S_i \le \frac{(\alpha_{high} + \theta_{high}/2)N_{sec}}{360} \quad (2)$$

and

$$R_i > (1 - \mu_{high})N_{ring} \quad (3)$$

the particle i and vertex j are located in the high layer sector. And when:

$$\frac{(\alpha_{low} - \theta_{low}/2)N_{sec}}{360} \le S_i \le \frac{(\alpha_{low} + \theta_{low}/2)N_{sec}}{360} \quad (4)$$

and

$$R_i > (1 - \mu_{low})N_{ring} \quad (5)$$

the particle i and vertex j are located in the low layer sector. Otherwise, the particle i and vertex j are located in the middle layer sector.

3.4. Tensioned zone and stressed zone

In the standard bending test of wood fracture mechanics [22] using rectangular planks, the fracture surface of the wood is divided into two parts: the ductile fracture zone and the brittle fracture zone. This phenomenon can also be observed in our bending experiment by using a branch with a diameter of 1 cm, as shown in Fig. 8. The shape of the ductile fracture zone on the rectangular wooden board is a rectangle, and the shape of the ductile fracture zone in the upper section of the branch is a fan shape or a fan ring. In future work, the finite element method can be used to calculate the deformation force experienced by each particle.

To simulate this phenomenon, our algorithm provides users with several parameters for setting the extent of the ductile fracture zone. $\alpha_{ductile}$ is the direction of the central axis of the ductile fracture zone. In Fig. 9, the position at which the magenta particles are located is subjected to a maximum tensile force; the red particle region is a ductile fracture region; and $\alpha_{ductile}$ can be determined, thereby producing the physically-based animation of a breaking branch. $\theta_{ductile}$ is the angle occupied of the ductile fracture zone. $\mu_{ductile}$ is the proportion occupied of concentric circles of the ductile fracture zone. L_D and P_D are the maximum length of the thorns on the ductile fracture zone and the probability of occurrence of thorns. The number of sectors on the cross-section is N_{sec}, and the sector position of the particle i is S_i. When:

$$\frac{(\alpha_{ductile} - \theta_{ductile}/2)N_{sec}}{360} \le S_i \le \frac{(\alpha_{ductile} + \theta_{ductile}/2)N_{sec}}{360} \quad (6)$$

and

$$R_i > (1 - \mu_{ductile})N_{ring} \quad (7)$$

Please cite this article as: L. Yang, M. Yang and G. Yang, Modeling fractures and cracks on tree branches, Computers & Graphics, https://doi.org/10.1016/j.cag.2019.03.006

Table 1
Physical-mechanical properties of wood [18,19].

Species	Case	Air-dried density (g/cm^3)	Drying shrinkage rate in the radial direction (%)	Drying shrinkage rate in the tangential direction (%)	Compressive strength along grain (MPa)	Bending strength (MPa)	Bending elastic modulus (GPa)	End hardness (N)	Anti-splitting strength (kgf/cm)
Juniperus viginiana L.	Fig. 10.(a)	0.53	3.1	4.7	25.0	49.0	4.6	4003	9.0
Juniperus Chinensis (L.) Ant.	Fig. 10.(b,c)	0.61	2.42	3.24	46.8	77.6	8.13	6252	6.7
Ailanthus altissima	Fig. 10.(d,e,f) Fig. 15.r	0.67	1.6	4.9	37.6	81.3	10.5	5374	19.1
Koelreuteria paniculata	Fig. 10.(g)	0.78	3.3	5.3	37.6	97.8	11.4	7286	22.0

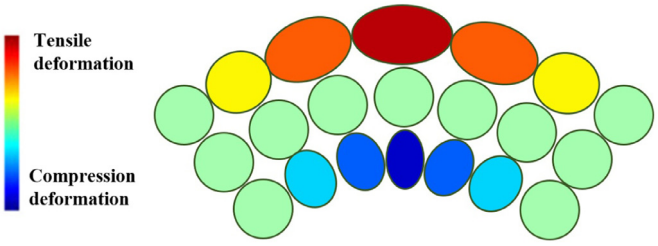

Fig. 9. Schematic diagram of particle deformation. When a branch was bent, the particles on the outer side in the bending direction are deformed by the tensile force, and the particles on the inner side are subjected to the pressure. (For interpretation of the references to color in this figure, the reader is referred to the web version of this article.)

Fig. 10. Broken branches of four tree species of about 1 cm in diameter. (a) Juniperus rigida S. et Z. (b,c) Juniperus Chinensis. The pith part is dark in color. (d,e,f) Ailanthus altissima. The fracture surface is relatively flat. (g) Koelreuteria paniculate.

the particle i is located in the ductile fracture zone. When the particles are in the ductile fracture zone, the patch of the particle may become a long thorn.

3.5. Wood thorns

Wood thorns are a prominent feature of a breaking branch. There are many kinds of conditions that cause wood thorns on the fracture surface of wood. For example, when branches are twisted, the individual wood fibers in the cross-section of branches are separated from each other, but the toughness of the wood fibers makes fibers continuous in the direction of the longitudinal axis. Wood thorns are formed after wood fibers break. Our work is to provide users with multiple parameters so as to quickly and realistically simulate branches with wood thorns. For different areas on branches: pith, heartwood, sapwood, phloem, ductile fracture zone and brittle fracture zone, specific parameters are set to control the length and probability of wood thorns. For each vertex on the fracture surface, a random value is generated. If the random value $Random() > P$, the additional height is added on the vertex j.

$$H_j += Random()L, Random() \in [0, 1] \tag{8}$$

where Random() is a function that generates a random value, L is the maximum length of thorns, P is the probability of occurrence of thorns, j is the vertex on the particle i, and H_j is the height of the vertex j.

According to the electron microscope scanning photographs of wood thorns as shown in [22], the artifact effect of wood thorns is represented by the shape of triangular pyramids. We splice irregular triangular pyramids on the top of 50–80% of slender hexahedron to get a more realistic wood thorn model.

3.6. Different tree species

Among forest plants in the world, there are more than 8,000 woody plants, of which more than 2000 are trees. Different tree species vary from morphological characteristics to internal structure and physical-mechanical properties, and their fracture effects are also very diverse. It is a very challenging task to establish the relation between the features of intuitive fracture effect, the common physical properties of wood and the arrangement of wood cells. In the experimental work of this paper, we collected 50 dry branches of four species with a diameter range of 0.5–5 cm. We bent and broke these branches and then observed the characteristics of the fracture surface. Our experiments suggest that the degree of delamination effect of the fracture surface has a linear relationship among the four physical-mechanical properties of wood (air-dried density, bending strength, bending elastic modulus and anti-splitting strength). When the measured values of the four physical properties of wood are lower, the larger the fracture surface area of the branches with a diameter of about 1 cm is, the more obvious the delamination effect is. As shown in Fig. 10, the area of the cypress-like branches (a–c) fracture surface are significantly larger than the branches of the other two species(d–g). The air-dried density and anti-cracking ability of the two species of Cypress trees tested in the experiment were less than the other two, as shown in Table 1. After experimental measurement, the ratio between the average fracture surface height and the branch radius of the four tree species branches are: 6.6835(Juniperus rigida S. et Z.), 3.025(Juniperus Chinensis (L.) Ant.), 0.7462(Ailanthus altissima), 0.5625(Koelreuteria paniculata).

$$h = (39.5271\rho - 0.2121R_B - 0.3708E_B - 0.2409R_C)D \tag{9}$$

Please cite this article as: L. Yang, M. Yang and G. Yang, Modeling fractures and cracks on tree branches, Computers & Graphics, https://doi.org/10.1016/j.cag.2019.03.006

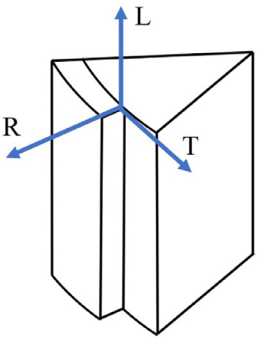

Fig. 11. Anisotropic material directions of wood: longitudinal direction, radial direction, and tangential direction.

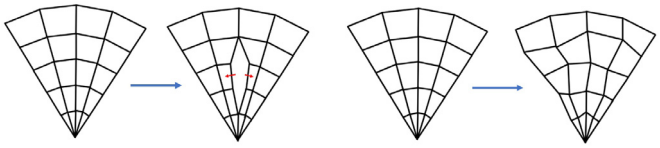

Fig. 12. (a) Generate a crack in the radial direction. (b) Add random displacement to vertices for simulating irregular shape of wood cells.

where h is the height of the fracture surface, D is the diameter of a tree branch, ρ is air-dried density, R_B is bending strength, E_B is bending elastic modulus, and R_C is anti-splitting strength. Eq. (8) shows that the ratio of height to the radius of the fracture surface of the branch has a strong correlation with several physical-mechanical properties of wood. It is feasible to apply the physical-mechanical properties of wood to characterize the fracture surface of branches.

A striking feature between the fracture surfaces of the branches of different tree species is the wood components of different colors and proportions on the cross-section, as shown in Fig. 10. We use the method in 3.2 to set the ratio of different materials.

4. Modeling cracks on tree branches

Dry shrinkage is an indispensable characteristic of wood. Several cracks are often seen on the broken branches or the cross-section of wood after horticultural pruning. The shape and propagation direction of these cracks has certain regularity. We propose a method for simulating cracks in the radial and tangential directions. Fig. 11 shows the anisotropic material directions of wood.

4.1. Cracks in the radial direction

When wood shrinks, cracks often occur at wood rays. The number and distribution of the wood ray of different tree species also differ a lot, so various dry cracking effects are produced. Users can set the shrinkage rate $\epsilon_{tangential}$, the angle at which the crack is located S_{crack}, the position of the concentric circle at the beginning of the crack R_{begin}, the position of the concentric circle at the end of the crack R_{end}, the depth of the crack D_{crack}, and the range of the shrinkage σ_{crack}, for creating a crack in the radial direction. As shown in Fig. 12(a), the sector to the left of the crack shrinks to the left, and the sector of the right shrinks to the right. The vertex j's position is P_j, the position of the vertex on the left of vertex j is $P_{j_{left}}$, the position of the vertex on the right of vertex j is $P_{j_{right}}$. When

$$(S_{crack} - \sigma_{crack}) \le S_j \le S_{crack} \tag{10}$$

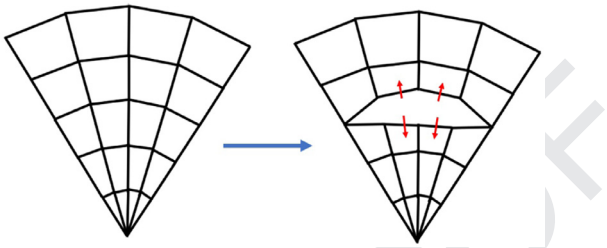

Fig. 13. Generate a crack in the tengential direction.

$$R_{begin} \le R_j \le R_{end} \tag{11}$$

$$(N_{layer} - D_{crack}) \le L_j \tag{12}$$

the vertex j is in the left region of the adding crack. So the position of vertex j should be translated to the left, and we calculate the shrinkage rate on the vertex j:

$$r_{j_{crack}} = |Rj - R_{begin} - 0.5(R_{end} - R_{begin})| \tag{13}$$

$$\epsilon_j = \frac{2\epsilon_{tangential}(D_{crack} - N_{layer} + L_j)|S_{crack} - S_j|r_{j_{crack}}}{D_{crack}\sigma_{crack}(R_{end} - R_{begin})} \tag{14}$$

$$P_j = (1 - \epsilon_j)P_j + \epsilon_j P_{j_{left}} \tag{15}$$

When Eq. (11), Eq. (12) and

$$S_{crack} \le S_j \le (S_{crack} + \sigma_{crack}) \tag{16}$$

the vertex j is in the right region of the adding crack. So the position of vertex j should be translated to the right, and we calculate the shrinkage rate on the vertex j:

$$P_j = (1 - \epsilon_j)P_j + \epsilon_j P_{j_{right}} \tag{17}$$

The distribution of wood rays is not regular, so we add radial and tangential random displacements to each vertex, as shown in Fig. 12(b).

4.2. Cracks in the tangential direction

Since annual rings are divided into early and late wood, in which the size and number of cells are different, cracks occur between the annual rings when wood shrinks. And because of the difference between pith, xylem and phloem cells, their boundaries often cause cracks. Our algorithm provides parameters for setting the shrinkage rate ϵ_{radial}, the position of the concentric circle R_{crack}, the position of the sector at the beginning of the crack S_{begin}, and the position of the sector at the end of the crack S_{end}, the depth of the crack D_{crack}, and the range of the shrinkage σ_{crack}, for creating a crack in the tangential direction. As shown in Fig. 13, the concentric circles on the outer side of the crack contract outwards, and those on the inner side contract inwards. The position of the outer vertex of vertex j is $P_{j_{outer}}$, and the position of the inner vertex of vertex j is $P_{j_{inner}}$. When Eq. (12) and

$$S_{begin} \le S_j \le S_{end} \tag{18}$$

$$(R_{crack} - \sigma_{crack}) \le R_j \le R_{crack} \tag{19}$$

the vertex j is in the inner region of the adding crack. So the position of vertex j should be translated to the inside, and we calculate the shrinkage rate on the vertex j:

$$s_{j_{crack}} = |Sj - S_{begin} - 0.5(S_{end} - S_{begin})| \tag{20}$$

Please cite this article as: L. Yang, M. Yang and G. Yang, Modeling fractures and cracks on tree branches, Computers & Graphics, https://doi.org/10.1016/j.cag.2019.03.006

Table 2
Main parameters used in our system and parameter-settings for the figures in this paper.

Name	Description	Range	Fig. 2.(g)	Fig. 15,r	Fig. 16,r	Fig. 17	Fig. 18,r	Fig. 19,r
D	The diameter of the brach	[0,500]	3	1	1	1	1	1
N_{ring}	The number of concentric circles on the cross-section	[3,400]	40	100	40	100	100	40
N_{sec}	The number of sectors on the cross-section	[10,1000]	40	100	40	100	100	40
φ	Angle of inclination	[0,90]	65	0	0	0	0	45
ν_{pith}	The propotion of the pith	[0,1]	0.05	0.05	0.05	0.05	0.05	0.05
$\nu_{heartwood}$	The propotion of the heartwood	[0,1]	0.05	0.45	0.75	0	0	0.3
ν_{phloem}	The propotion of the phloem	[0,1]	0.05	0.125	0.05	0.05	0.05	0.1
λ_{phloem}	Set the roughness of the phloem part of fracture surface	[0,5]	0.2	0.06	0.02	0.07	0.05	1
β_{phloem}	Set the roughness of the phloem part of fracture surface	[1,10000]	460	2000	460	200	100	200
$\lambda_{sapwood}$	Set the roughness of the sapwood part of fracture surface	[0,5]	0.2	0.02	0.02	0.07	1	1
$\beta_{sapwood}$	Set the roughness of the sapwood part of fracture surface	[1,10000]	460	400	460	200	5000	200
$\lambda_{heartwood}$	Set the roughness of the heartwood part of fracture surface	[0,5]	0.2	0.02	0.02	0.07	1	1
$\beta_{heartwood}$	Set the roughness of the heartwood part of fracture surface	[1,10000]	460	200	460	200	5000	200
h_{high}	The ratio of the relative heights of the high layer to the radius	[0,20]	1	0	0.5	1.8	3	0
α_{high}	The direction of the high layer sectors	[0,360]	10	0	0	0	0	0
θ_{high}	The angle of the high layer sectors	[0,360]	60	0	180	150	60	0
μ_{high}	The proportion of rings of the high layer sectors	[0,1]	1	0	1	0.6	0.2	0
h_{low}	The ratio of the relative heights of the low layer to the radius	[−20,0]	−1	0	−0.3	0	0	−4
α_{low}	The direction of the low layer sectors	[0,360]	170	180	135	180	180	180
θ_{low}	The angle of the low layer sectors	[0,360]	60	0	30	0	0	80
μ_{low}	The proportion of rings of the low layer sectors	[0,1]	1	0	0.2	0	0	0.25
L_D	The maximum length of the thorns on the ductile fracture zone	[0,40]	0	0.2	0	5	0	0
P_D	The probability of occurrence of thorns on the ductile fracture zone	[0,1]	0	0.35	0	0.1	0	0
$\alpha_{ductile}$	The direction of the ductile fracture zone	[0,360]	0	0	0	0	0	0
$\theta_{ductile}$	The angle of the ductile fracture zone	[0,360]	0	150	0	150	0	0
$\mu_{ductile}$	The proportion of rings of the ductile fracture zone	[0,1]	0	0.5	0	0.6	0	0

Table 3
Performance. Generation time is the required time to generate a new model after each parameter modification.

Case	N_{ring}	N_s	Generation time(s)
Fig. 16.r	40	40	0.018
Fig. 15.r	100	100	0.085
–	200	200	0.354

$$\epsilon_j = \frac{2\epsilon_{tangential}(D_{crack} - N_{layer} + L_j)s_{j_{crack}}|R_{crack} - R_j|}{D_{crack}\sigma_{crack}(R_{end} - R_{begin})} \tag{21}$$

$$P_j = (1 - \epsilon_j)P_j + \epsilon_j P_{j_{inner}} \tag{22}$$

And when Eqs. (12) and (18)

$$R_{crack} \le R_j \le (R_{crack} + \sigma_{crack}) \tag{23}$$

the vertex j is in the outer region of the adding crack. So the position of vertex j should be translated to the outside, and we calculate the shrinkage rate on the vertex j:

$$P_j = (1 - \epsilon_j)P_j + \epsilon_j P_{j_{outer}} \tag{24}$$

5. Implementation and results

Our system is implemented in C++, using OpenGL and GLSL for rendering. All results were generated on a computer with a 2.50 GHz Intel i7-6500U CPU processor and 8GB RAM, and rendered with an Intel(R) HD Graphics 520 GPU.

We present Table 2 for a clearer description of the settings of some of the main parameters and the effects of them. Some other parameters with similar functions are not shown here, but the actual complex effects are generated by 2-3 Perlin noise and 3-4 white noise controlled by multiple parameters.

Table 3 shows the performance of our method. When we set the sector value to 40 and the concentric circle value to 40, we can design and adjust the fracture surface of a branch model in real time, as the simulation result shown in Fig. 16. For the more refined model such as Fig. 15, we set the sector number to 100 and the concentric circle value to 100. It takes about 0.085 s to get the final model effect after adjusting the parameters each time. So we usually design the model roughly now with $N_{ring} = 40$ and $N_s = 40$; finally set $N_{ring} = 100$ and $N_s = 100$; and adjust some details such as the number and shape of the long thorn.

When users want to quickly model a realistic broken branch, they can set 26–32 parameters according to the design flow shown in Fig. 2. The values of each parameter need to be adjusted manually about 3–5 times to achieve a desirable result. Users can get the final model in 10 min. Nevertheless, our method cannot get exactly the same model as the real object, but it is more efficient and its result is close to the real effect than the previous method.

Fig. 14 shows the results produced by different values of λ and β. When the value of λ and β are both higher, the cross-section is covered with dense thorns. When the λ and the β are both lower values, the fracture surface is like a soft wave.

There is no obvious stratification of the branches in Fig. 15(right), but three regions with different roughness can be perceived on the cross-section. The branches in Fig. 16(right) have obvious stratification. This effect can be easily achieved by setting the nine parameters given in Chapter 3.3.

Fig. 17 shows the simulation of a broken branch with obvious tensioned zone and stressed zone.Fig. 18 shows the simulation of a broken fresh branch. Because the fiber toughness of fresh young branches is greater than that of dry branches, it shows the effect of full fiber spines. Fig. 19 shows the simulation of the broken branch on the tree.

The simulation result with some random distortions added is more realistic than the original regular cracks, as shown in Fig. 20.

Fig. 21 shows the simulation of the cross-section of wood with many cracks. To simulate such effect, first of all, some analysis and statistics of cracks need to be done manually. Also, such analysis and statistics in future work can be accomplished by image processing and machine vision. Firstly, all radial cracks in the cross section are divided into large cracks, medium cracks, and small

Please cite this article as: L. Yang, M. Yang and G. Yang, Modeling fractures and cracks on tree branches, Computers & Graphics, https://doi.org/10.1016/j.cag.2019.03.006

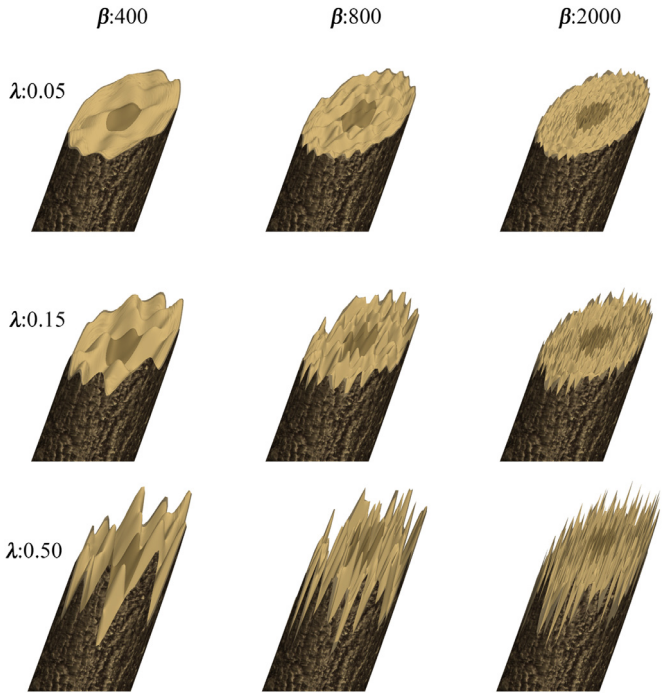

Fig. 14. Comparison of the fracture surface of branches with different roughness. We change the values of λ and β to adjust Perlin noise in Eq. (1). From left to right, β is set to 400,800,2000. From top to bottom, λ is set to 0.05,0.15,0.5.

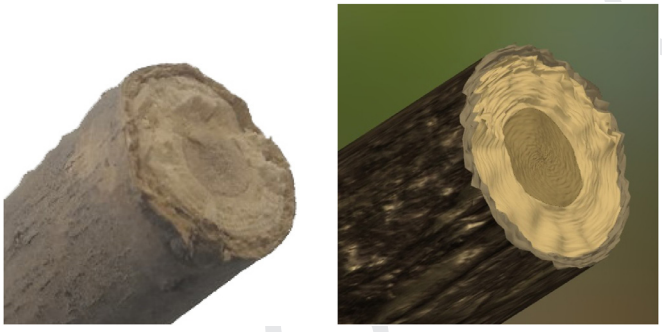

Fig. 15. A photograph and a simulation result of a broken branch of Ailanthus altissima with a diameter of about 1 cm. It can be observed from the photograph that the fracture surface has a side which is rougher than the other side, and the phloem is more uneven than the xylem.

Fig. 16. A photograph and a simulation result of a broken branch. The fracture surface is clearly divided into sectors occupying a relatively high height of about 180°, occupying a medium-height sector of about 150°, and occupying a sector of a lower height of about 30°.

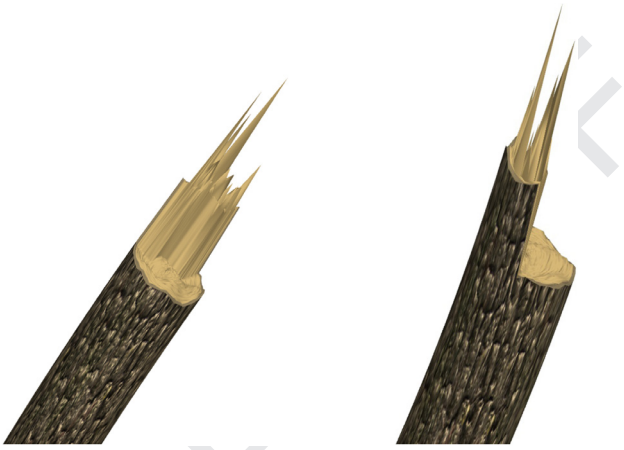

Fig. 17. Simulation results of the broken right branch in Fig. 8.

Fig. 18. A photograph and a simulation result of a broken branch of Amygdalus triloba f. multiplex. The fracture surface consists of many long thorns.

Fig. 19. A photograph and a simulation result of a broken branch.

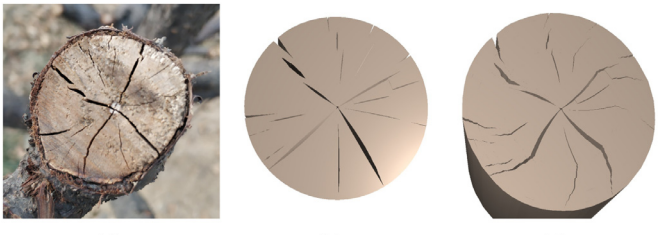

Fig. 20. Photograph and simulation result of cracks on the branch's cross-section of Amygdalus triloba f. multiplex. (b) The simulation result without random displacement on vertices.

Please cite this article as: L. Yang, M. Yang and G. Yang, Modeling fractures and cracks on tree branches, Computers & Graphics, https://doi.org/10.1016/j.cag.2019.03.006

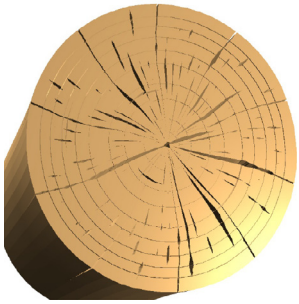

Fig. 21. A simulation result of the cracks on the branch's cross-section.

cracks according to the size of the cracks. Average angle between the cracks of each group is counted after manual measurement. Finally, based on these statistics, you can get the range of parameters in Section 4.1, and then randomly set the parameters required.

6. Conclusions and future work

We have proposed a user-controllable branch fracture simulation method in this paper. The added model design principles from the knowledge of wood science and fracture mechanic capture a wide range of real-world fracture shapes. Our approach reproduces realistic breaking effects in branches of different tree species. There are possible future research directions for the more in-depth study of wood fracture patterns in order to provide graphics applications, such as artistic design, scientific visualization or wood science education, etc.

Our approach cannot generate physically-based animations of tree branches breaking. We would like to combine position based dynamics [30,31] into our work to generate real-time interactive animations of tree branches breaking in future work. The using of the PBD method enables more precise handling of the collisions made by long fiber thorns in animations, contributing to more complex animation effects. We'll use the method of extracting bones [32] to extend the particle representation of our working branches to 3-dimensional tree models that have irregular shapes, such as extremely curved or multi-forks.

The knots in branches destroy the symmetry of wood, change the direction of wood fiber extension, bring twisted annual rings, curved texture, and affect the physical-mechanical properties of wood. The cambium of the knots is connected to the cambium of a trunk. The knots and the forks bring complexity to the modeling of the internal structure of wood. There is a need to design a method to handle the internal particle structure of wood with tree knots or tree forks in the future.

In future work, we will experiment on the fracture effect of branches of more tree species to obtain new insights and better modeling methods. More experiments can be performed to study the differences in the effects of breaking branches of different diameter. For the fracture effect of some large diameter trunks, it is difficult to carry out real experiments for observations or reconstruct the tree trunk fractures that have mutually obstructed and twisted wood fibers by 3D scanning technology. Thus, the detection and processing of wood fiber distortion, breakage, and collision in the process of tree breaking is the key problem to be solved in animation of tree breaking.

Since wood moisture is an important factor affecting the performance of wood, and most of the experimental materials used in this paper are dry branches, the experiment on the effect of fresh branch fracture can enlarge the range of existing results. Extending this work to the fracture simulation of wood furniture, and wood crafts is also a meaningful task that would benefit more practical applications.

Acknowledgments

This work has been supported by The Fundamental Research Funds for the Central Universities (2017JC10, 2015ZCQ-XX), Beijing Social Science Fund (17YTC030), and National Natural Science Foundation of China (61402038, 61502109).

References

[1] Weber J, Penn J. Creation and rendering of realistic trees. In: Proceedings of the 22nd annual conference on computer graphics and interactive techniques, SIGGRAPH '95. New York, NY, USA: ACM; 1995. p. 119–28. ISBN 0-89791-701-4. doi:10.1145/218380.218427.
[2] Xu H, Gossett N, Chen B. Knowledge-based modeling of laser-scanned trees.. In: Proceedings of the SIGGRAPH sketches; 2005. p. 124.
[3] Livny Y, Yan F, Olson M, Chen B, Zhang H, ElSana J. Automatic reconstruction of tree skeletal structures from point clouds. In: Proceedings of the ACM transactions on graphics (TOG), 29. ACM; 2010. p. 151.
[4] Livny Y, Pirk S, Cheng Z, Yan F, Deussen O, Cohen-Or D, et al. Texture-lobes for tree modelling. In: Proceedings of the ACM SIGGRAPH 2011 Papers, SIGGRAPH '11. New York, NY, USA: ACM; 2011. p. 53:1–53:10. ISBN 978-1-4503-0943-1. doi:10.1145/1964921.1964948.
[5] Xie K, Yan F, Sharf A, Deussen O, Huang H, Chen B. Tree modeling with real tree-parts examples. IEEE Trans Vis Comput Graph 2016;22(12):2608–18.
[6] Pirk S, Niese T, Deussen O, Neubert B. Capturing and animating the morphogenesis of polygonal tree models. ACM Trans Graph (TOG) 2012;31(6):169:1–169:10. doi:10.1145/2366145.2366188.
[7] Kratt J, Spicker M, Guayaquil A, Fiser M, Pirk S, Deussen O, et al. Woodification: user-controlled cambial growth modeling. Comput Graph Forum 2015;34(2):361–72. doi:10.1111/cgf.12566.
[8] Diener J, Rodriguez M, Baboud L, Reveret L. Wind projection basis for real-time animation of trees. Research Report. INRIA; 2008. https://hal.inria.fr/inria-00328122.
[9] Quigley E, Yu Y, Huang J, Lin W, Fedkiw R. Real-time interactive tree animation. IEEE Trans Vis Comput Graph 2018;24(5):1717–27. doi:10.1109/TVCG.2017.2661308.
[10] Yang M, Wu E. Approach for physically-based animation of tree branches impacting by raindrops. J Softw 2011;22(8):1934–47.
[11] Wang B, Zhao Y, Barbič J. Botanical materials based on biomechanics. ACM Trans Graph (TOG) 2017;36(4):135:1–135:13. doi:10.1145/3072959.3073655.
[12] Pirk S, Jarzabek M, Hädrich T, Michels DL, Palubicki W. Interactive wood combustion for botanical tree models. ACM Trans Graph (TOG) 2017;36(6):197:1–197:12. doi:10.1145/3130800.3130814.
[13] O'Brien JF, Bargteil AW, Hodgins JK. Graphical modeling and animation of ductile fracture. In: Proceedings of ACM SIGGRAPH 2002. ACM Press; 2002. p. 291–4. http://graphics.cs.berkeley.edu/papers/Obrien-GMA-2002-08/.
[14] Pfaff T, Narain R, de Joya JM, O'Brien JF. Adaptive tearing and cracking of thin sheets. ACM Trans Graph (TOG) 2014;33(4):110:1–110:9. doi:10.1145/2601097.2601132.
[15] Chen Z, Yao M, Feng R, Wang H. Physics-inspired adaptive fracture refinement. ACM Trans Graph (TOG) 2014;33(4):113.
[16] Desbenoit B, Galin E, Akkouche S. Modeling cracks and fractures. Vis Comput 2005;21(8-10):717–26.
[17] Zhao R, Yu Y. Wood material science (in Chinese). China Forestry Publishing House; 2003.
[18] Physical and mechanical properties of wood from major tree species in China(in Chinese). China Forestry Publishing House; 1982.
[19] Jiang Z, Peng Z. Wood properties of the global important tree species (in Chinese). Science Press; 2001.
[20] Yao X. Structure of main chinese woods-scanning electron microscope (in Chinese). China Forestry Publishing House; 1988.
[21] Vasic S, Smith I, Landis E. Finite element techniques and models for wood fracture mechanics. Wood Sci Technol 2005;39(1):3–17.
[22] Shao Z, Wang F. The fracture mechanics of plant materials; 2018.
[23] Khennane A, Khelifa M, Bleron L, Viguier J. Numerical modelling of ductile damage evolution in tensile and bending tests of timber structures. Mech Mater 2014;68:228–36.
[24] Fei B, Zhang D. China Wood Industry 2003;17(3):000007–12.
[25] Xu W. Research on wood chip shear and impact of the fracture characteristics based on fractal theory (Ph.D. thesis) (in chinese). Northeast Forestry University; 2012.
[26] Sun J, Hu Y, Wang F, Han T. Fractional analysis of wood fracture surface based on image processing (in chinese). Chin J Sci Instrum 2013;34(12):2818–23.
[27] Jackson MD, Xu H, Duran-Nebreda S, Stamm P, Bassel GW. Topological analysis of multicellular complexity in the plant hypocotyl. Elife 2017;6:e26023.
[28] Montenegro-Johnson TD, Stamm P, Strauss S, Topham AT, Tsagris M, Wood AT, et al. Digital single-cell analysis of plant organ development using 3DCellAtlas. Plant Cell 2015. tpc–15.

[29] Sapala A, Runions A, Routier-Kierzkowska A-L, Gupta MD, Hong L, Hofhuis H, et al. Why plants make puzzle cells, and how their shape emerges. eLife 2018;7:e32794.
[30] Müller M, Heidelberger B, Hennix M, Ratcliff J. Position based dynamics. J Vis Commun Image Represent 2007;18(2):109–18.
[31] Macklin M, Müller M, Chentanez N, Kim T-Y. Unified particle physics for real-time applications. ACM Trans Graph (TOG) 2014;33(4):153.
[32] Au OK-C, Tai C-L, Chu H-K, Cohen-Or D, Lee T-Y. Skeleton extraction by mesh contraction. In: Proceedings of the ACM transactions on graphics (TOG), 27. ACM; 2008. p. 44.

Please cite this article as: L. Yang, M. Yang and G. Yang, Modeling fractures and cracks on tree branches, Computers & Graphics, https://doi.org/10.1016/j.cag.2019.03.006